RSC Advances

PAPER

View Article Online
View Journal | View Issue

Cite this: *RSC Adv.*, 2018, **8**, 40647

Enhanced hydrogen storage properties of $1.1MgH_2–2LiNH_2–0.1LiBH_4$ system with $LaNi_5$-based alloy hydrides addition

Wang Zhao, [a] Yuanfang Wu,[b] Ping Li, *[a] Lijun Jiang*[b] and Xuanhui Qu [a]

Significant improvements in the hydrogen sorption properties of the Li–Mg–N–H system have been achieved by adding a small amount of $LiBH_4$. Herein, the hydrogen storage properties of the $1.1MgH_2–2LiNH_2–0.1LiBH_4$ system are further enhanced by addition of $LaNi_5$-based ($LaNi_{3.8}Al_{0.75}Mn_{0.45}$, $LaNi_{4.5}Mn_{0.5}$, $LaNi_4Co$) alloy hydrides. The refinement of the Li–Mg–B–N–H particles and the metathesis reaction are facilitated by adding $LaNi_5$-based alloy hydrides during the ball milling process. The addition of $LaNi_5$-based alloy hydrides can enhance the hydrogen sorption kinetics, reduce the dehydrogenation temperature and promote a more thorough dehydrogenation of the Li–Mg–B–N–H system. The $LaNi_5$-based alloy hydrides are involved in hydrogen de/hydrogenation reaction. Among the three alloys, $LaNi_{4.5}Mn_{0.5}$ makes the most obvious improvement on the reaction kinetics, and the dehydrogenation peak temperature is reduced by 12 °C, while the activation energy is reduced by 11% with 10 wt% $LaNi_{4.5}Mn_{0.5}$ addition. The weakening of the N–H bond and the homogeneous distribution of the $LaNi_5$-based alloy hydrides in the Li–Mg–B–N–H composite have important roles in the reduction of the desorption barrier and the kinetics enhancement.

Received 31st August 2018
Accepted 22nd November 2018

DOI: 10.1039/c8ra07279e

rsc.li/rsc-advances

1. Introduction

Hydrogen is an ideal fuel in terms of the concept of comprehensive clean-energy. However, hydrogen storage is still a major technical barrier for its practical application.[1,2] To solve this problem, materials with high gravimetric and volumetric hydrogen capacity and fast de/hydrogenation kinetics under moderate temperature and pressure conditions need to be obtained.[3–5]

Metal–N–H hydrogen storage systems have attracted considerable attention in the past few years as alternative hydrogen storage materials to the traditional metal hydrides.[6–10] Among the studied materials, the Li–Mg–N–H system comprised of LiH and $Mg(NH_2)_2$ or $LiNH_2$ and MgH_2, exhibits a relatively high capacity of 5.6 wt% and good reversibility at moderate operation temperatures, which can dehydrogenate under 0.1 MPa at 90 °C by thermodynamic calculation.[8] It is therefore regarded as a promising candidate for hydrogen storage if the high kinetics barrier of hydrogen sorption can be overcome.[6,7]

$LiBH_4$ is an effective additive to enhance hydrogen sorption properties of the $Mg(NH_2)_2$–2LiH system.[11–13] By analyzing the dehydrogenation reaction process of the ternary $LiBH_4$–$2LiNH_2$–MgH_2 composite, a new self-catalyzing strategy for enhancing the kinetics of hydrogen storage in complex hydride composites has been discovered.[14] The stoichiometry of this ternary complex hydride system has a significant impact on the hydrogen storage property.[15–19] A small amount of $LiBH_4$ addition can increase the hydrogen absorption and desorption kinetics of $Mg(NH_2)_2$–LiH (0.1 : 1 : 2, molar ratio) by a factor of three.[19] But the hydrogen sorption kinetics is still choke point hindering good thermodynamics and impedes the practical application of Li–Mg–B–N–H system. To further improve the hydrogen storage behavior, various transition metal-based additives including nanoscale metal particles, metal oxides and metal hydrides were investigated.[20–26] It was found that the additives of nanoscale Co and Ni particles lowered the hydrogen releasing temperature at least 75–100 °C in the major hydrogen decomposition step, while other additives (Fe, Cu, Mn) acted as catalysts and increased the rate at which hydrogen was released.[20] Various nanoscale metal oxide catalysts, such as CeO_2, TiO_2, Fe_2O_3, Co_3O_4, and SiO_2, were also added to the $LiBH_4$–$2LiNH_2$–MgH_2 system.[21] It was found that the metal oxides could enhance the kinetics and decrease the temperatures of the hydrogen desorption reactions in low temperature region. Some metal hydrides, such as $Ti_3Cr_3V_4$ and $ZrFe_2$ hydrides, have shown significantly catalytic effects on the de/hydrogenation characteristic of $Mg(NH_2)_2$–LiH.[22,23] For the Li–Mg–B–N–H system, significant improvements in the hydrogen sorption properties have been achieved with the addition of $ZrCoH_3$ or $ZrFe_2$.[24–26] However, $ZrCoH_3$ is difficult to

[a]*Institute for Advanced Materials and Technology, University of Science and Technology Beijing, Beijing 100083, China. E-mail: ustbliping@126.com*
[b]*Institute of Energy Materials and Technology, GRIMAT Engineering Institute Co., Ltd., Beijing 101407, China. E-mail: jlj@grinm.com*

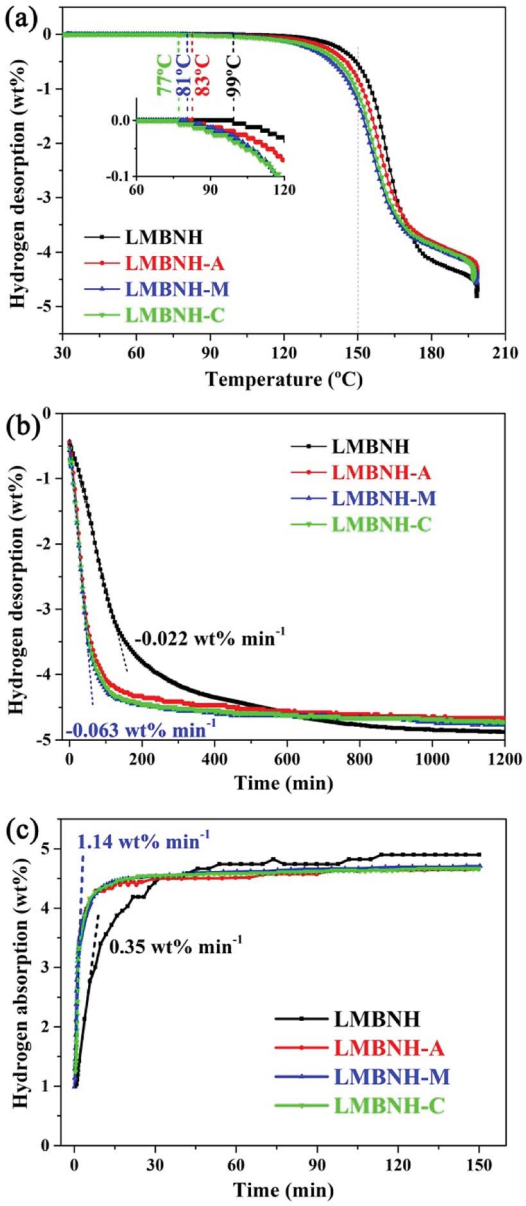

Fig. 1 (a) TPD curves of the Li–Mg–B–N–H samples with and without $LaNi_5$-based alloy hydrides at a heating rate of 1 °C min^{-1}. The inset is the partial enlargement. (b) Isothermal dehydrogenation curves under 0.03 MPa at 150 °C of the Li–Mg–B–N–H samples with and without $LaNi_5$-based alloy hydrides. (c) Isothermal rehydrogenation curves under 7 MPa at 150 °C of the Li–Mg–B–N–H samples with and without $LaNi_5$-based alloy hydrides.

dehydrogenate for the characteristic of rather low plateau pressure (about 50 Pa at 150 °C for $ZrCoH_3$),[27] and $ZrFe_2$ is difficult to hydrogenate at 180 °C under 7 MPa H_2 for the characteristic of rather high plateau pressure (*ca.* 70 MPa at 22 °C for $ZrFe_2$).[28] Thus, $ZrCoH_3$ and $ZrFe_2$ would not participate in de/hydrogenation process, resulting in capacity loss.

In our earlier work, the cycle performance and the hydrogen capacity fading mechanism of the $1.1MgH_2$–$2LiNH_2$–$0.1LiBH_4$ system with $LaNi_{4.5}Mn_{0.5}$ alloy addition was investigated.[29] $LaNi_{4.5}Mn_{0.5}$ with moderate platform pressure ranging from 0.5 to 1 MPa at 150 °C can absorb and release hydrogen in synchronization with Li–Mg–B–N–H system.[30] Herein, $LaNi_5$-based alloys were added to the $2LiNH_2$–$1.1MgH_2$–$0.1LiBH_4$ composite to enhance the hydrogen storage properties. Three alloys, $LaNi_{3.8}Al_{0.75}Mn_{0.45}$, $LaNi_{4.5}Mn_{0.5}$ and $LaNi_4Co$, with plateau pressures range from 0.05 to 3 MPa at 150 °C,[30–32] were added to this complex hydride system respectively. It is noteworthy that the $LaNi_5$-based alloy can absorb or desorb hydrogen in de/hydrogenation condition of $1.1MgH_2$–$2LiNH_2$–$0.1LiBH_4$ system, which will contribute to hydrogen storage capacity of the composite materials. And the $LaNi_5$-based alloy with larger hardness can facilitate refinement of the Li–Mg–B–N–H particles, which would help improve the kinetics. In this work, the hydrogen storage properties of $1.1MgH_2$–$2LiNH_2$–$0.1LiBH_4$ system with $LaNi_5$-based alloy hydrides addition were investigated and the catalytic mechanism was discussed.

2. Experimental

2.1 Synthesis of composite

The starting materials $LiNH_2$ and $LiBH_4$ (95% purity, Sigma-Aldrich) were used as received without purification. The MgH_2 was home-made by ball-milling Mg powder (99% purity, Trillion Metal) under 4 MPa H_2 pressure for 60 h, and then it was hydrogenated under 5 MPa H_2 pressure at 400 °C for three times to obtain high purity MgH_2 (>95% purity).

The $LaNi_5$-based intermetallic compounds ($LaNi_{3.8}Al_{0.75}Mn_{0.45}$, $LaNi_{4.5}Mn_{0.5}$ and $LaNi_4Co$) were prepared by magnetic levitation melting from La, Ni, Al, Mn and Co (>99% purity, Trillion Metal) under argon atmosphere. The alloys were re-melted three times and annealed in evacuated quartz tubes at 1000 °C for 8 hours, and then quenched in the water. The annealed alloy was hydrogenated for pulverizing to −500 mesh powder under 5 MPa H_2 pressure at ambient temperature.

The mixture of MgH_2, $LiNH_2$ and $LiBH_4$ with molar ratio of 1.1 : 2 : 0.1 was loaded into a stainless steel vial for high-energy ball-milling using Spex-8000 apparatus. In order to prevent the decomposition of the mixture, 4 MPa H_2 was filled. The weight ratio of stainless steel ball to powder was 20 : 1 and the total milling time was 36 hours. Then 10 wt% $LaNi_{3.8}Al_{0.75}Mn_{0.45}$, $LaNi_{4.5}Mn_{0.5}$ and $LaNi_4Co$ alloy hydrides were added to the as-milled Li–Mg–B–N–H and milled for 12 hours, which were denoted as LMBNH-A, LMBNH-M, LMBNH-C, respectively. The reference sample Li–Mg–B–N–H without $LaNi_5$-based alloy addition was prepared in the same manner, which was denoted as LMBNH.

2.2 Characterization

The temperature programmed desorption (TPD) and isothermal dehydrogenation kinetics was measured using a Sieverts-type apparatus, and approximately 0.5 g of sample was used in each measurement. During the heating procedure of the isothermal dehydrogenation test, the samples were subjected to a hydrogen pressure of 4 MPa to prevent premature decomposition. Differential scanning calorimetry (DSC) measurements were performed on a Netzsch DSC 409 unit. About 40 mg of samples were heated at a heating rate of 3, 5, 8 and 10 °C min^{-1}

Table 1 Hydrogen desorption capacities at different stages of the Li–Mg–B–N–H samples with and without $LaNi_5$-based alloy hydrides

		Hydrogen desorption capacity (wt%)					
		TPD			Isothermal		
Samples	H content of alloy	150 °C	200 °C	Theoretical value of 200 °C	200 min	1200 min	Theoretical value of 1200 min
LMBNH	—	0.55	4.81	4.81	3.12	4.88	4.88
LMBNH-A	1.24	0.84	4.52	4.45	4.16	4.67	4.52
LMBNH-M	1.55	1.28	4.57	4.48	4.33	4.77	4.55
LMBNH-C	1.57	1.10	4.51	4.49	4.31	4.73	4.55

under Ar atmosphere. The gas generated in the heating process was monitored by a mass spectrometer (MS). The structural analyses of the composites were carried out by XRD characterization employing X'pert Pro MPD diffractometer with Cu Kα radiation at 40 kV and 40 mA. The samples were covered with polyimide films to isolate the air. The IR absorption spectrum was collected in diffuse reflectance infrared Fourier transform mode at a resolution of 4 cm^{-1}, and the sample was mixed with paraffine in an appropriate proportion in order to isolate air. The microstructural characterizations of the samples were done employing scanning electron microscope (SEM, Hitachi model S4800). All the sample handling procedures in this work were performed in an argon-filled glove-box with H_2O and O_2 concentration below 1 ppm.

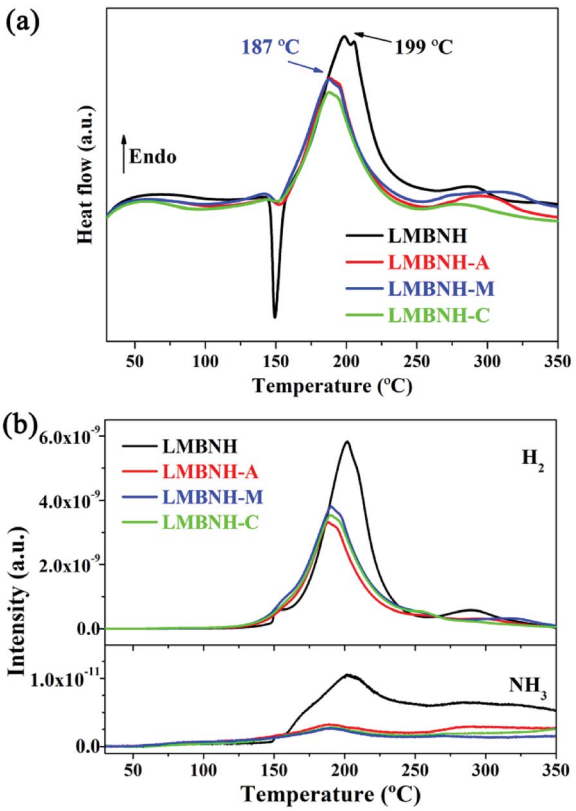

Fig. 2 (a) DSC curves and (b) MS monitoring of H_2 and NH_3 generated during DSC at heating rate of 5 °C min^{-1} from 30 °C to 350 °C of the Li–Mg–B–N–H sample with and without $LaNi_5$-based alloy hydrides.

3. Results and discussion

3.1 Hydrogen storage properties

The dehydrogenation performance was measured for comparison of the effects induced by the addition of $LaNi_{3.8}Al_{0.75}Mn_{0.45}$, $LaNi_{4.5}Mn_{0.5}$ and $LaNi_4Co$. The TPD curves obtained at a heating rate of 1 °C min^{-1} are shown in Fig. 1(a). The initial dehydrogenation temperatures as determined by the change in the hydrogen desorption capacity significantly decrease with the addition of $LaNi_5$-based alloy hydrides. The dehydrogenation kinetics are enhanced dramatically at the same time and the most significant improvement in desorption kinetics is LMBNH-M. For the pristine sample and the sample added with 10 wt% $LaNi_{3.8}Al_{0.75}Mn_{0.45}$, $LaNi_{4.5}Mn_{0.5}$ and $LaNi_4Co$, the initial dehydrogenation temperature is 99 °C, 83 °C, 81 °C and 77 °C, respectively. That is, the initial temperatures of the samples added with $LaNi_5$-based alloy hydrides are reduced by 18–22 °C. Moreover, they falls into the operating temperature range of proton exchange membrane fuel cells.[33,34] When the temperature rising to 150 °C, the hydrogen desorption capacities are significantly improved by addition of $LaNi_5$-based alloys, especially LMBNH-M (Table 1). Due to the larger densities and the smaller capacities of $LaNi_5$-based alloys compared with the pristine sample, there are capacity losses (ranging from 0.32 to 0.36 wt%) of the total hydrogen capacities for the samples added alloy hydrides. The capacity losses can be reduced by optimizing the composite composition. However, it is interesting that the samples added alloy hydrides release more hydrogen by calculating the theoretical capacity. Taking LMBNH-M as an example, its practical capacity is 4.57 wt% while theoretical capacity is 4.48 wt%. The theoretical capacity is calculated with reference to the hydrogen content of alloy and the total capacity of the Li–Mg–B–N–H sample. It may mean that the addition of $LaNi_5$-based alloys promote a more complete dehydrogenation of the Li–Mg–B–N–H composite.

The isothermal desorption/absorption curves obtained at 150 °C are shown in Fig. 1(b) and (c). The addition of $LaNi_5$-based alloy hydrides significantly enhance the hydrogen desorption and absorption kinetics. Similar to TPD results, LMBNH-M shows best isothermal desorption kinetics. By analyzing the tangent slope of the linear parts for hydrogen desorption, the rate constant for LMBNH-M is estimated to be 0.063 wt% min^{-1}, about three times that for LMBNH (0.022 wt% min^{-1}). In the rehydrogenation step (Fig. 1(c)),

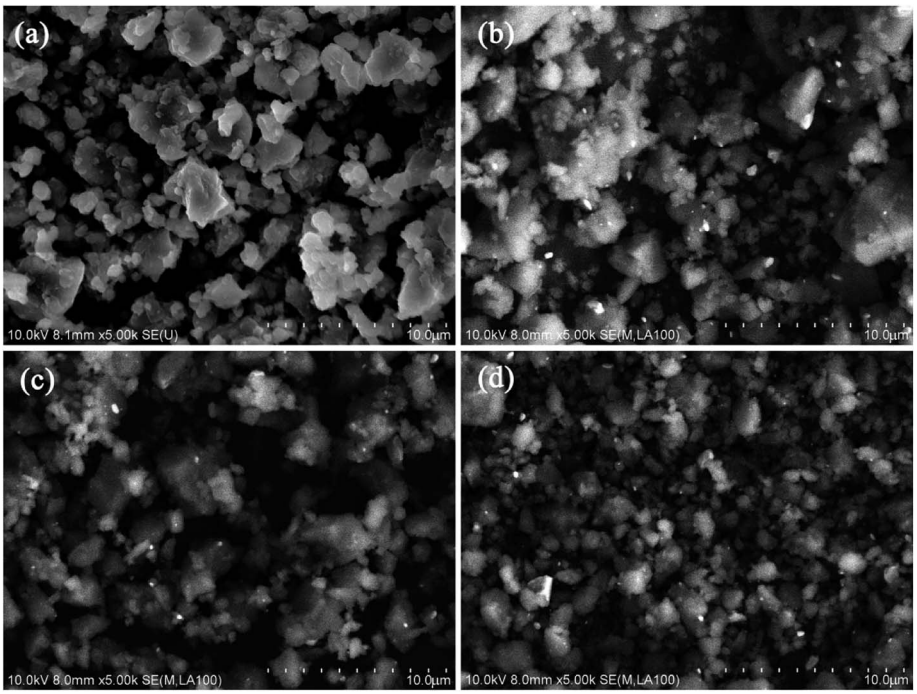

Fig. 3 SEM images of (a) LMBNH, (b) LMBNH-A, (c) LMBNH-M, (d) LMBNH-C after ball milling.

LMBNH-M also exhibits better performance than the other samples. At the hydrogen pressure of 7 MPa, hydrogen capacity can reach 4.50 wt% in 20 minutes for LMBNH-M, while only 4.03 wt% for LMBNH. All the samples can fully rehydrogenation in 150 minutes. The rehydrogenation rate constant for LMBNH-M is estimated to be 1.14 wt% min^{-1} by the same approach, which is also about three times that for LMBNH (0.35 wt%-min^{-1}). The hydrogen desorption capacities at different times are shown in Table 1. Compared with theoretical values, more hydrogen are released during isothermal desorption process with addition of alloy hydrides. Combining TPD and isothermal dehydrogenation kinetics, it can be concluded that, the $LaNi_5$-based alloys improve the dehydrogenation performance and promote a more thorough dehydrogenation of the Li–Mg–B–N–H composite.

The DSC curves of the Li–Mg–B–N–H sample with and without $LaNi_5$-based alloy hydrides which were measured at 5 °C min^{-1} from 30 °C to 350 °C under argon atmosphere are shown in Fig. 2(a). The broad endothermic peaks in the temperature range of 180–200 °C can be viewed as superposition of two peaks, which correspond to the two hydrogen desorption reaction reported by Yang in eqn (1) and (2) respectively.[14]

$$2Li_4BN_3H_{10} + 3MgH_2 \rightarrow 3Li_2Mg(NH)_2 + 2LiBH_4 + 6H_2 \quad (1)$$

$$Mg(NH_2)_2 + 2LiH \rightarrow Li_2Mg(NH)_2 + 2H_2 \quad (2)$$

The quaternary hydride $Li_4BN_3H_{10}$ should be formed by the reaction of $LiNH_2$ and $LiBH_4$ during sample preparation.[14] The endothermic peak temperature of LMBNH-M is 187 °C, 12 °C lower than that of LMBNH, which agrees with TPD result. The endothermic peaks are narrower than the pristine sample as well, reflecting a fast rate of dehydrogenation near the peak temperature.[35] It can be clearly found that there is a sharp exothermic peak for LMBNH at 150 °C, which coincides with the metathesis reaction (eqn (3)).[25]

$$2LiNH_2 + MgH_2 \rightarrow Mg(NH_2)_2 + 2LiH \quad (3)$$

However, the exothermic peaks for the samples added $LaNi_5$-based alloy hydrides become weak, which implies that the metathesis reaction of eqn (3) has been largely complete during ball milling process. In other words, more efficient ball milling is achieved by addition of $LiBH_4$ and $LaNi_5$-based alloy hydrides, which promotes the proceeding of the metathesis reaction from $LiNH_2/MgH_2$ to $Mg(NH_2)_2/LiH$. And no heating or high hydrogen pressure of about 10 MPa is required.[18,25,36]

The temperature dependence of hydrogen and ammonia release from the Li–Mg–B–N–H sample with and without $LaNi_5$-based alloy hydrides was investigated by mass spectrometer (Fig. 2(b)), which was coupled with the DSC measurement. It could be found that the positions of the hydrogen signal peaks correspond well with those of endothermic peaks in the DSC curves. As consistent with the DSC results, the hydrogen desorption peak temperature reduces by 12 °C with the addition of $LaNi_5$-based alloy hydrides. The DSC and MS results demonstrate that the $LaNi_5$-based alloys facilitate the hydrogen desorption reaction and thereby accelerate the dehydrogenation kinetics. The monitoring of ammonia generation indicates that ammonia evolution can be inhibited during dehydrogenation process with the addition of $LaNi_5$-based alloy hydrides. By roughly estimating the signal intensity, the ammonia release

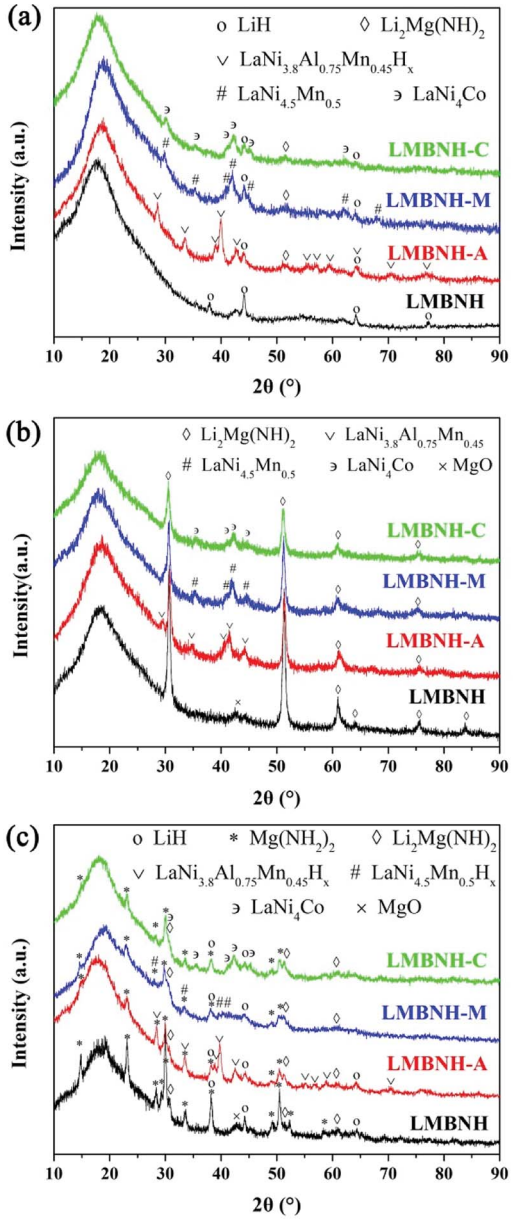

Fig. 4 XRD patterns of the Li–Mg–B–N–H samples with and without $LaNi_5$-based alloy hydrides (a) after ball milling, (b) after dehydrogenation, (c) after incomplete rehydrogenation for 30 min. The diffraction peaks originated by polyimide film are within 15–25°, far from the main peak region of the samples.

is reduced by about 75%. As we have known, the increase of LiH content can inhibit the release of ammonia for the Li–Mg–N–H system.[37,38] Some other hydrides, such as KH,[9] RbH,[10] Li_3AlH_6,[39] and $Mg(BH_4)_2$–$Mg(NH_2)_2$ compound,[40] have also been proved to decrease the emission of the ammonia. Here, $LaNi_5$-based alloy hydrides may have the same positive effects. However, the ammonia inhibition mechanism needs to be further clarified.

3.2 Phase and microstructure characterization

Fig. 3 shows the SEM images of the Li–Mg–B–N–H samples with and without $LaNi_5$-based alloy hydrides after ball milling. For all samples, the particles are relatively uniform in size and some agglomerations can be found. As can be seen in Fig. 3(b–d), there are some uniformly distributed nano-sized bright particles that should be $LaNi_5$-based alloy in the matrix. The Li–Mg–B–N–H particles in the samples with $LaNi_5$-based alloy hydrides are smaller than that in the pristine sample. Owing to the larger hardness, the alloy particles can act as micro-balls in the ball milling process to further grind the Li–Mg–B–N–H material, resulting in more efficient ball milling. The refinement of the material particles will increase the surface area, reduce the diffusion distance of hydrogen atoms, and then lead to a faster reaction kinetics.[41] The homogeneous distribution of the $LaNi_5$-based alloy hydrides in the Li–Mg–B–N–H matrix is critical for the catalysis effect. A closer look in Fig. 3 reveals that the $LaNi_{4.5}Mn_{0.5}$ alloy has a smaller particle size than the other two alloys. In other words, the $LaNi_{4.5}Mn_{0.5}$ alloy has the better dispersibility, which may be one of the reasons for the better desorption kinetics.

To understand the phase composition, samples collected after ball milling were characterized using XRD method (Fig. 4(a)). $LiBH_4$ cannot be identified mainly because its content was too low. LiH is observed in the samples, indicating the occurrence of the metathesis reaction (eqn (3)) during the ball milling process, which generated $Mg(NH_2)_2$ and LiH. $Mg(NH_2)_2$ was easily transferred to the amorphous form, which has been reported in other similar works.[12,40,42,43] Besides, after energetic ball milling, the particle sizes of MgH_2 and $LiNH_2$ would be refined. Therefore, three factors, including grain refinement, metathesis reaction and amorphization behavior, together lead to the inability of the original materials MgH_2 and $LiNH_2$ to be identified. According to the DSC results, the metathesis reaction is promoted by addition of $LaNi_5$-based alloy hydrides, and the content of LiH should increase as a matter of course. However, the introduction of $LaNi_5$-based alloy hydrides facilitates pulverization and amorphization of the material in the ball-milling process, so the diffraction intensities of LiH become lower. The alloy phase can be identified, and the broadened and weakened peaks indicate the occurrence of grain refinement and amorphous phase in the grains due to ball-milling as well. The added alloy hydrides released hydrogen during the transfer and storage on account of the relatively high plateau pressure for LMBNH-M and LMBNH-C, even though the samples were prepared by ball milling under 4 MPa H_2 pressure. For all the samples added $LaNi_5$-based alloy hydrides, the dehydrogenation product $Li_2Mg(NH)_2$ can be found even after ball milling, which means the dehydrogenation reaction can occur more easily in the presence of $LaNi_5$-based alloy.

As shown in Fig. 4(b), for the sample after dehydrogenation at 150 °C for 20 hours, there is mainly a dehydrogenation product $Li_2Mg(NH)_2$, which was proposed in early reports.[14,18] The alloy phase ($LaNi_{3.8}Al_{0.75}Mn_{0.45}$, $LaNi_{4.5}Mn_{0.5}$ and $LaNi_4Co$) can be detected in the corresponding samples, which manifests that the alloys are involved in the dehydrogenation reaction. In order to clarify the phase composition during hydrogen absorption, the samples after dehydrogenation were hydrogenated under hydrogen pressure of 7 MPa at 150 °C for 30 min.

For the samples after incomplete rehydrogenation (Fig. 4(c)), the main phases are LiH and $Mg(NH_2)_2$, and there is a little residual $Li_2Mg(NH)_2$. The alloy hydrides are formed after absorbing hydrogen for LMBNH-A and LMBNH-M. For LMBNH-C, the $LaNi_4Co$ remains the state of alloy, which might release hydrogen again during the transfer and storage for its high plateau pressure. No newly formed phase can be identified from these results in the sample with $LaNi_5$-based alloy hydrides addition (Fig. 4), which is an indication of no interaction between $LaNi_5$-based alloy hydrides and Li–Mg–B–N–H composite.

3.3 Catalytic mechanism

Employing the DSC measurements to obtain the endothermic peak temperatures at various heating rate (3, 5, 8 and 10 °C min^{-1}, respectively), four Kissinger plots were draw to estimate the apparent activation energies for the Li–Mg–B–N–H samples with and without $LaNi_5$-based alloy hydrides (Fig. 5). According to Kissinger's theory,[44] activation energy E_a can be determined by using eqn (4).

$$\ln(\beta/T^2) = \ln(AR/E_a) - E_a/RT \quad (4)$$

In the above equation, T is the peak temperature, A is the pre-exponential factor, β is the heating rate, E_a is the activation energy, and R is the gas constant. The activation energy can be calculated from the slope of the fitted line (Fig. 5(a)). As we can see, the Kissinger plots have good linearity for all samples. The dehydrogenation activation energies are found to be 76.0, 70.1, 67.4 and 68.7 kJ mol^{-1} for LMBNH, LMBNH-A, LMBNH-M and LMBNH-C, respectively. In other words, about 8–11% reduction in the activation energy is achieved by the addition of $LaNi_5$-based alloy hydrides. This means the addition of $LaNi_5$-based alloy hydrides lowers desorption barrier, which is responsible for the reduction of the initial hydrogen desorption temperature and the enhancement of the hydrogen desorption kinetics for Li–Mg–B–N–H composite. Part of the reasons for the decrease of activation energy may be that $LaNi_5$-based alloy hydrides refine the matrix particles and increase hydrogen diffusion channels. Moreover, the $LaNi_5$-based alloys with better hydrogen storage properties can be hydrogenated or dehydrogenated prior to Li–Mg–B–N–H composite, in other words, the alloys may transfer hydrogen atom to/from the interface between alloy and Li–Mg–B–N–H, which maybe work as hydrogen pumps.[45,46]

The FTIR spectroscopy was used to understand the influence of the $LaNi_5$-based alloy hydrides on the structure of the Li–Mg–B–N–H composite (Fig. 6). As can be seen in Fig. 6(a), for the samples after ball milling, the absorbance at 3326 and 3268 cm^{-1} suggests the existence of $Mg(NH_2)_2$ which is not detected in XRD patterns, and the characteristic N–H vibration of $LiNH_2$ at 1562 cm^{-1} has also been found. This indicates an incomplete metathesis reaction which is in consistency with the XRD results. For the samples with addition of $LaNi_5$-based alloy hydrides, the weak and broad absorbance at 3168 cm^{-1} indicates the formation of the ternary imide $Li_2Mg(NH)_2$, which has been found in the XRD results. That is to say, with addition of $LaNi_5$-based alloys, the dehydrogenation reaction has occurred during the ball milling process. For the samples after incomplete rehydrogenation (Fig. 6(b)), the typical N–H vibrations at 3326 and 3268 cm^{-1} of $Mg(NH_2)_2$ remain unchanged. And the N–H vibration of $LiNH_2$ at 1562 cm^{-1} disappears while the absorbance emerged at 1568 cm^{-1} appears which represents $Mg(NH_2)_2$. The broad absorbance at 3168 cm^{-1} represents $Li_2Mg(NH)_2$ that is not fully hydrogenated.

More importantly, a slight shifting of the N–H vibration to the lower wavenumbers can be found (the absorption peaks at 3268 and 1562 cm^{-1} in Fig. 6(a), 3268 and 1568 cm^{-1} in Fig. 6(b)), which indicates a weakening of the N–H bonds. The N–H weakening acts as an important role in the reduction of desorption barrier and the kinetics enhancement.[8,9,24,39,47] This bond weakening effect may be attributed to the interaction between the lone electron pair of the nitrogen atom and the hybrid orbitals of transition metal elements in the $LaNi_5$-based alloy.[24,26,48,49] Besides, the homogenously distributed $LaNi_5$-based alloys in the Li–Mg–B–N–H matrix can refine the particles and enhance the hydrogen atom diffusion, which significantly

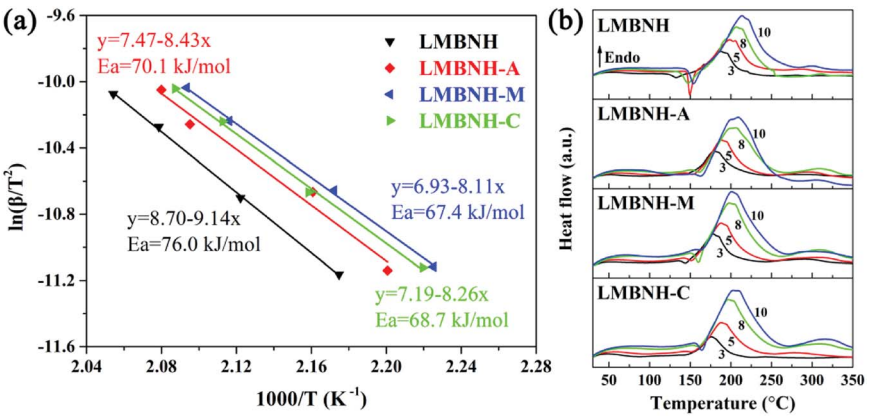

Fig. 5 (a) Kissinger plots of the Li–Mg–B–N–H samples with and without $LaNi_5$-based alloy hydrides, (b) DSC curves for the Li–Mg–B–N–H samples with and without $LaNi_5$-based alloy hydrides at heating rate of 3, 5, 8, 10 °C min^{-1} from 30 °C to 350 °C.

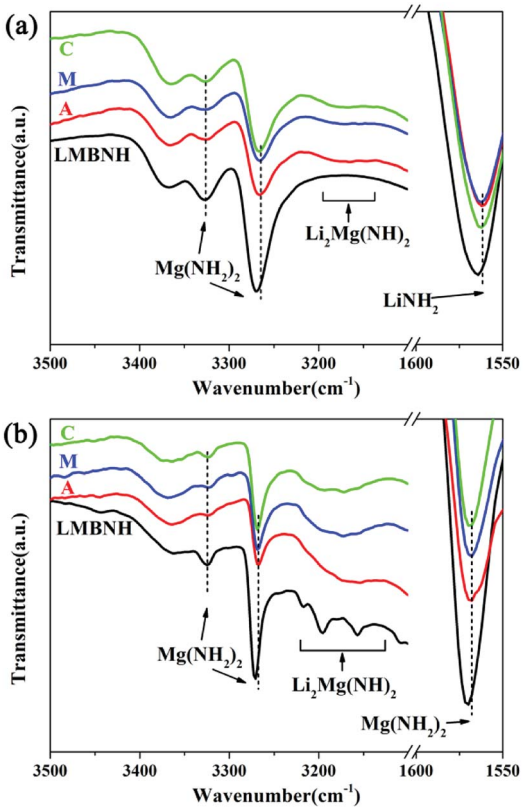

Fig. 6 FTIR spectra of the Li–Mg–B–N–H samples with and without $LaNi_5$-based alloy hydrides (a) after ball milling, (b) after incomplete rehydrogenation for 30 min.

accelerate the reaction kinetics. The two aspects described above could be the main reasons for the improved hydrogen storage performance for the Li–Mg–B–N–H added $LaNi_5$-based alloy hydrides.

4. Conclusions

The hydrogen storage properties of $1.1MgH_2$–$2LiNH_2$–$0.1LiBH_4$ system are enhanced by addition of $LaNi_5$-based alloy ($LaNi_{3.8}Al_{0.75}Mn_{0.45}$, $LaNi_{4.5}Mn_{0.5}$, $LaNi_4Co$) hydrides. The refinement of the Li–Mg–B–N–H particles and the metathesis reaction are facilitated by addition of $LaNi_5$-based alloy hydrides during ball milling process. The $LaNi_5$-based alloy hydrides could enhance the hydrogen sorption kinetics, reduce the dehydrogenation temperature and promote a more thorough dehydrogenation of the Li–Mg–B–N–H system. The $LaNi_5$-based alloy hydrides are involved in de/hydrogenation reaction. Among the three alloys, $LaNi_{4.5}Mn_{0.5}$ makes the most obvious improvement on the reaction kinetics. For the sample added $LaNi_{4.5}Mn_{0.5}$, the dehydrogenation peak temperature lowers by 12 °C, the activation energy reduces by 11% and the kinetics of hydrogen desorption/absorption are about three times as fast as the pristine system. The weakening of the N–H bond and the homogeneous distribution of the $LaNi_5$-based alloy hydrides in the Li–Mg–B–N–H composite act as important roles in the reduction of desorption barrier and the enhancement of sorption kinetics.

Conflicts of interest

There are no conflicts to declare.

Acknowledgements

This work was supported by the National Natural Science Foundation of China (Grant No. 51471054).

References

1 L. Schlapbach and A. Züttel, *Nature*, 2001, **414**, 353–358.
2 T. He, P. Pachfule, H. Wu, Q. Xu and P. Chen, *Nat. Rev. Mater.*, 2016, **1**, 16059.
3 M. B. Ley, L. H. Jepsen, Y. S. Lee, Y. W. Cho, J. M. B. Colbe, M. Dornheim, M. Rokni, J. O. Jensen, M. Sloth, Y. Filinchuk, J. E. Jørgensen, F. Besenbacher and T. R. Jensen, *Mater. Today*, 2014, **17**, 122–128.
4 Q. Lai, M. Paskevicius, D. A. Sheppard, C. E. Buckley, A. W. Thornton, M. R. Hill, Q. Gu, J. Mao, Z. Huang, H. K. Liu, Z. Guo, A. Banerjee, S. Chakraborty, R. Ahuja and K. F. Aguey-Zinsou, *ChemSusChem*, 2015, **8**, 2789–2825.
5 Y. Liu, Y. Yang, M. Gao and H. Pan, *Chem. Rec.*, 2016, **16**, 189–204.
6 P. Chen, Z. Xiong, J. Luo, J. Lin and K. L. Tan, *Nature*, 2002, **420**, 302.
7 Z. Xiong, G. Wu, J. Hu and P. Chen, *Adv. Mater.*, 2004, **16**, 1522–1525.
8 Z. Xiong, J. Hu, G. Wu, P. Chen, W. Luo, K. Cross and J. Wang, *J. Alloys Compd.*, 2005, **398**, 235–239.
9 J. H. Wang, T. Liu, G. T. Wu, W. Li, Y. F. Liu, C. M. Araujo, R. H. Scheicher, A. Blomqvist, R. Ahuja, Z. T. Xiong, P. Yang, M. X. Gao, H. G. Pan and P. Chen, *Angew. Chem., Int. Ed.*, 2009, **48**, 5828–5832.
10 C. Li, Y. F. Liu, R. J. Ma, X. Zhang, Y. Li, M. X. Gao and H. G. Pan, *ACS Appl. Mater. Interfaces*, 2014, **6**, 17024–17033.
11 J. Yang, A. Sudik, D. J. Siegel, D. Halliday, A. Drews, R. O. Carter III, C. Wolverton, G. J. Lewis, J. W. A. Sachtler, J. J. Low, S. A. Faheem, D. A. Lesch and V. Ozolins, *J. Alloys Compd.*, 2007, **446**, 345–349.
12 J. Hu, E. Weidner, M. Hoelzel and M. Fichtner, *Dalton Trans.*, 2010, **39**, 9100–9107.
13 M. U. Niemann, S. S. Srinivasan, A. Kumar, E. K. Stefanakos, D. Y. Goswami and K. McGrath, *Int. J. Hydrogen Energy*, 2009, **34**, 8086–8093.
14 J. Yang, A. Sudik, D. J. Siegel, D. Halliday, A. Drews, R. O. Carter III, C. Wolverton, G. J. Lewis, J. W. A. Sachtler, J. J. Low, S. A. Faheem, D. A. Lesch and V. Ozolins, *Angew. Chem., Int. Ed.*, 2008, **47**, 882–887.
15 G. J. Lewis, J. W. A. Sachtler, J. J. Low, D. A. Lesch, S. A. Faheem, P. M. Dosek, L. M. Knight, L. Halloran, C. M. Jensen, J. Yang, A. Sudik, D. J. Siegel, C. Wolverton, V. Ozolins and S. Zhang, *J. Alloys Compd.*, 2007, **446**, 355–359.
16 A. Sudik, J. Yang, D. Halliday and C. Wolverton, *J. Phys. Chem. C*, 2008, **112**, 4384–4390.

17 A. Sudik, J. Yang, D. J. Siegel, C. Wolverton, R. O. Carter III and A. R. Drews, *J. Phys. Chem. C*, 2009, **113**, 2004–2013.
18 J. Hu, M. Fichtner and P. Chen, *Chem. Mater.*, 2008, **20**, 7089–7094.
19 J. Hu, Y. Liu, G. Wu, Z. Xiong, Y. S. Chua and P. Chen, *Chem. Mater.*, 2008, **20**, 4398–4402.
20 S. S. Srinivasan, M. U. Niemann, J. R. Hattrick-Simpers, K. McGrath, P. C. Sharma, D. Y. Goswami and E. K. Stefanakos, *Int. J. Hydrogen Energy*, 2010, **35**, 9646–9652.
21 H. Yuan, X. Zhang, Z. Li, J. Ye, X. Guo, S. Wang, X. Liu and L. Jiang, *Int. J. Hydrogen Energy*, 2012, **37**, 3292–3297.
22 J. Wang, Z. Li, H. Li, J. Mi, F. Lü, S. Wang, X. Liu and L. Jiang, *Rare Met.*, 2010, **29**, 621–624.
23 V. Shukla, A. Bhatnagar, S. K. Pandey, R. R. Shahi, T. P. Yadav, M. A. Shaz and O. N. Srivastava, *Int. J. Hydrogen Energy*, 2015, **40**, 12294–12302.
24 X. Zhang, Z. Li, F. Lv, H. Li, J. Mi, S. Wang, X. Liu and L. Jiang, *Int. J. Hydrogen Energy*, 2010, **35**, 7809–7814.
25 J. Hu, A. Pohl, S. Wang, J. Rothe and M. Fichtner, *J. Phys. Chem. C*, 2012, **116**, 20246–20253.
26 V. Shukla, A. Bhatnagar, P. K. Soni, A. K. Vishwakarma, M. A. Shaz, T. P. Yadav and O. N. Srivastava, *Phys. Chem. Chem. Phys.*, 2017, **19**, 9444–9456.
27 M. Devillers, M. Sirch, S. Bredendiek-Kämper and R. D. Penzhorn, *Chem. Mater.*, 1990, **2**, 255–262.
28 R. B. Sivov, T. A. Zotov and V. N. Verbetsky, *Int. J. Hydrogen Energy*, 2011, **36**, 1355–1358.
29 W. Zhao, L. Jiang, Y. Wu, J. Ye, B. Yuan, Z. Li, X. Liu and S. Wang, *J. Rare Earths*, 2015, **33**, 783–790.
30 H. Nakamura, Y. Nakamura, S. Fujitani and I. Yonezu, *J. Alloys Compd.*, 1997, **252**, 83–87.
31 Y. Jiang, X. Liu, L. Jiang, S. Wang and H. Yang, *Rare Met.*, 2006, **25**, 204–208.
32 C. E. Lundin, F. E. Lynch and C. B. Magee, *J. Less-Common Met.*, 1977, **56**, 19–37.
33 J. Yang, A. Sudik, C. Wolverton and D. J. Siegel, *Chem. Soc. Rev.*, 2010, **39**, 656–675.
34 S. J. Peighambardoust, S. Rowshanzamir and M. Amjadi, *Int. J. Hydrogen Energy*, 2010, **35**, 9349–9384.
35 H. Cao, G. Wu, Y. Zhang, Z. Xiong, J. Qiu and P. Chen, *J. Mater. Chem. A*, 2014, **2**, 15816–15822.
36 W. Luo and S. Sickafoose, *J. Alloys Compd.*, 2006, **407**, 274–281.
37 Z. Xiong, G. Wu, J. Hu, P. Chen, W. Luo and J. Wang, *J. Alloys Compd.*, 2006, **417**, 190–194.
38 M. Aoki, T. Noritake, Y. Nakamori, S. Towata and S. Orimo, *J. Alloys Compd.*, 2007, **446**, 328–331.
39 H. Cao, Y. Zhang, J. Wang, Z. Xiong, G. Wu, J. Qiu and P. Chen, *Dalton Trans.*, 2013, **42**, 5524–5531.
40 Y. Zhang, Z. Xiong, H. Cao, G. Wu and P. Chen, *Int. J. Hydrogen Energy*, 2014, **39**, 1710–1718.
41 Y. Liu, K. Zhong, K. Luo, M. Gao, H. Pan and Q. Wang, *J. Am. Chem. Soc.*, 2009, **131**, 1862–1870.
42 B. Li, Y. Liu, J. Gu, M. Gao and H. Pan, *Chem.–Asian J.*, 2013, **8**, 374–384.
43 H. Pan, S. Shi, Y. Liu, B. Li, Y. Yang and M. Gao, *Dalton Trans.*, 2013, **42**, 3802–3811.
44 H. E. Kissinger, *Anal. Chem.*, 1957, **29**, 1702–1706.
45 G. Liang, J. Huot, S. Boily, A. Van Neste and R. Schulz, *J. Alloys Compd.*, 1999, **291**, 295–299.
46 P. Chen and M. Zhu, *Mater. Today*, 2008, **11**, 36–43.
47 C. Liang, Y. Liu, Z. Wei, Y. Jiang, F. Wu, M. Gao and H. Pan, *Int. J. Hydrogen Energy*, 2011, **36**, 2137–2144.
48 R. R. Shahi, T. P. Yadav, M. A. Shaz and O. N. Srivastva, *Int. J. Hydrogen Energy*, 2010, **35**, 238–246.
49 H. Zheng, Y. Wang and G. Ma, *Eur. Phys. J. B*, 2002, **29**, 61–69.